Physics 357: Diode Laser Spectroscopy

Eliseu Antonio Kloster Filho, Jacob Garcia
(Dated: December 5th, 2023)

Saturated absorption spectroscopy (SAS) and resonant Faraday rotation were investigated in the context of a Rb vapor cell. The D_2 transitions of the two abundant isotopes were observed, and saturated absorption was observed for the hyperfine splitting of ^{85}Rb's F'. Resonant Faraday rotation was observed in the presence of an applied magnetic field, although the hypothesis of a purely linear dependence on it could not be supported by this experiment.

I. INTRODUCTION

When a beam of light interacts with any material, some of the photons get reflected, and some of the photons get absorbed by it. In the process of absorption, atoms move from lower-energy states to higher-energy states, since they receive a surplus of energy from the photons. However, only certain wavelengths of light are capable of being absorbed because the internal structure of the atoms is formed by discrete energy levels. In particular, different elements (and isotopes) have their own unique energy levels arrangement, which means the intensity of absorption varies with the frequency of the light that is being absorbed. The "absorption spectrum" can thus be used to uniquely identify each element. The study of such spectra is called absorption spectroscopy (in contrast with other types of spectroscopy), and it is the main focus of our experiment. Through the technique of saturated absorption spectroscopy (SAS), the first part of our experiment aimed to reduce the Doppler broadening from a Rb cell and achieve saturated absorption. The second part of our experiment sought to measure resonant Faraday rotation and show a linear dependence to the applied B-field.

A. Rubidium Atomic Structure

The ground-state electronic configuration of rubidium involves a closed single 5s valence electron. The first excited state moves this electron up to the 5p orbital. There are two stable rubidium isotopes: 85Rb (72 percent abundance) and 87Rb (28 percent abundance).

Energy levels are described by using spectroscopic notation $^{2S+1}L'_J$, providing the angular quantum numbers of a state. S is the spin quantum number, L' is the angular momentum quantum number (i.e. single electron states are described by S, P, D, F..., matching one-to-one with the series of orbital quantum numbers, L = 0,1,2,3,...), and J = L + S is the total angular momentum quantum number. The first excited state gives $S = \frac{1}{2}$ and L = 1. This produces a total angular momentum quantum number $J = \frac{1}{2}$ or $J = \frac{3}{2}$, giving two excited states $^2P_{\frac{1}{2}}$ and $^2P_{\frac{3}{2}}$.

Due to the interaction between the nuclear spin and the electron, hyperfine energy splitting of otherwise degenerate energy levels occurs [1]. This depends on F = I + J which includes the nuclear spin. Each of the hyperfine (F) energy levels contains 2F + 1 magnetic sublevels [2]. Our experiment is concerned with the D_2 transition ($5S_{\frac{1}{2}} \implies 5P_{\frac{3}{2}}$). This transition occurs at 780.241 209 686(13) nm for ^{87}Rb and at 780.241 368 271(27) nm for ^{85}Rb [2][3].

B. Absorption Spectrum

Saturated absorption spectroscopy is a technique used to measure the narrow-line atomic spectral features of an atomic vapor with large Doppler broadening $\Delta v_{Dopp} \sim 1GHz$ [4]. It employs two overlapping pump and probe laser beams directed into a vapor cell. Because gaseous atoms have a random distribution of velocities, not all will be on resonance with an incident beam. Only Atoms moving toward the probe beam with a specific longitudinal velocity related to the laser frequency $v = v_0 - \Delta v$ will absorb it [4]. These atoms will be unaffected by the pump beam pointing in the opposite direction. If the laser frequency is $v = v_0$, atoms with zero longitudinal velocity will absorb the probe beam [4][5]. These atoms will also be on-resonance with the pump beam which has enough power to keep a majority of them in the excited state. Because of the depletion of the atoms in the ground state, the absorption of the probe beam decreases in the presence of a strong pump beam [5]. This causes the sharpened peak which is observed in the probe beam's transmission spectra at the resonance frequency.

If the atoms have a single ground state and two excited ones, and the separation of the excited states was less than the Doppler width, then a "cross-over resonance" peak in the transmission spectra would appear. This peak occurs at the frequency $(v_1 + v_2)/2$ where v_1 and v_2 are the two resonance frequencies [4].

C. Faraday Rotation

When considering the mechanisms behind Faraday rotation here, the medium's effect on incident fields must be considered. The light incident on the Rb cell is linearly polarized, and it decomposes into two opposite-handed, circularly polarized fields, $\hat{\sigma}_+$ and $\hat{\sigma}_-$. Each has its own index of refraction n_+ and n_- respectively [6]. For simplicity's sake these polarizations will be expressed as the

real part of the following:

$$\hat{\sigma}_{\pm} = \hat{x} \pm i\hat{y} \tag{1}$$

This allows $\hat{x}$ to be described as the following linear combination:

$$\hat{x} = \frac{1}{2}(\hat{\sigma}_{+} + \hat{\sigma}_{-}) \tag{2}$$

For a given value of z, in vacuum, the resultant E-field is therefore:

$$\vec{E}_{\pm}(z,t) = E_0(\hat{\sigma}_{+} + \hat{\sigma}_{-})e^{i(kz-\omega t)} \tag{3}$$

The field of incident light (z=0) is then described as:

$$\vec{E}(0,t) = 2E_0\hat{x}e^{-i\omega t} \tag{4}$$

When passing through the medium, $\vec{E}_{\pm}(z,t)$ must pick up phase factors related to the indices of refraction $n_{\pm}$. This introduces

$$k_{\pm} = kn_{\pm} \tag{5}$$

as the modified wave number. Assuming no attenuation, an incident field propagating through a sample of length L will be become

$$\vec{E}(L,t) = E_0(e^{i(n_{+}kL-\omega t)}\hat{\sigma}_{+} + e^{i(n_{-}kL-\omega t)}\hat{\sigma}_{-}) \tag{6}$$

For simple case of no attenuation, $\vec{E}(L,t)$ can be written as the following [6]:

$$\vec{E}(L,t) = 2E_0\left(\hat{x}\cos\Delta\theta - \hat{y}\sin\Delta\theta\right)\exp i\left(k\frac{n_{+}+n_{-}}{2}L - \omega t\right) \tag{7}$$

This expresses a linearly polarized wave whose polarization has been rotated through the Faraday rotation angle $\Delta\theta$ by [6]

$$\Delta\theta = k\left(\frac{n_{+}-n_{-}}{2}\right)L \tag{8}$$

This specific case can be described more generally. When polarized light propagates through a medium under the influence of a constant magnetic field parallel to its axis, the left- and right-handed components acquire different phase factors, causing the plane of polarization to be rotated by a small angle $\Delta\phi$ depending on the distance L of propagation. This effect was first discovered by Faraday in 1845 (hence the name Faraday Rotation) and to obtain a theoretical prediction, it suffices to use a semi-classical model in which the electron is bound to the nucleus by a spring of constant $K = m\omega_0^2$ (the Lorentz oscillator model). If put under the influence of a strong external field $B_0\hat{z}$ and the weak transverse EM wave generated by light $\vec{E}_w e^{i(kz-\omega t)}$ ($E_w = B_w \ll B_0$).

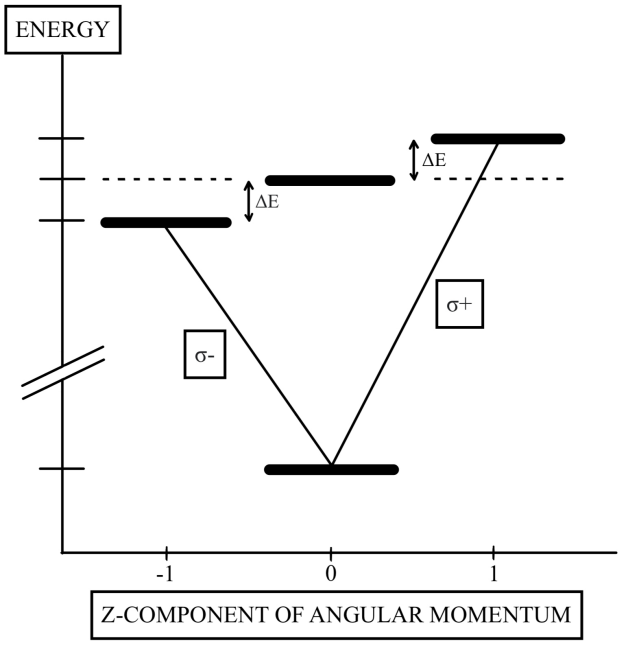

FIG. 1: The atomic system explored in this experiment. There is a non-degenerate ground state and an excited one with three sublevels, split by an external magnetic field for the transition ${}^1S_0 \implies {}^1P_1$. Adapted from van Baak [6].

$$\omega_B = \frac{eB_0}{mc} \tag{9}$$

$$\omega_p = \sqrt{\frac{4\pi Ne^2}{m}} \tag{10}$$

$$V_B = \frac{e}{2mc^2}\frac{\omega^2\omega_p^2}{(\omega_0^2-\omega^2)^2 - \omega^2\omega_B^2} \tag{11}$$

$$\Delta\phi \approx V_B B_0 L \tag{12}$$

The model atomic system for this experiment is a gas of independent atoms, and each has a non-degenerate ground state and excited state [6]. Van Baak identified this system as showing a "normal" Zeeman effect. He notes that in the presence of an external magnetic field $\vec{B} = B_0\hat{x}$, the higher energy sublevels split as shown in fig. 1. The z-projections ($m_F = \pm 1$) of the total angular momentum F=1 for the simplest transition ${}^1S_0 \implies {}^1P_1$ undergo the following energy shift [6]:

$$\Delta E = \pm B_0\frac{e\hbar}{2m_e} \tag{13}$$

Therefore each of the circular polarizations, σ_{+} and σ_{-}, will interact with their own transition, and each polarization will have its own index of refraction [6].

D. Applications of Diode Laser Spectroscopy

The spectroscopy technique utilized in this lab does not restrict itself to just the pure study of atomic structures. On the contrary: diode laser spectroscopy finds applications in a diversity of different fields, including in medicine, process monitoring, and automobile industry. Here, we briefly describe another two in more detail.

1. Remote sensing: The absorption intensity becomes more and more attenuated as we decrease the concentration of the element being analyzed. Similarly, the spectrum can also be affected by the length of the optical path that light travels. These two general principles are more precisely described by Beer Lambert's law, which is the basic principle behind various trace gas sensing technologies. Two of the most common techniques in this field are scanned-wavelength direct absorption spectroscopy (DAS) and scanned-wavelength modulation spectroscopy (WMS) [7].

2. Astronomy: Astronomers analyze absorption and emission spectra all the time, so it should not be surprising that diode laser spectroscopy can be useful in this area. More specifically, Jennings has shown that infrared spectroscopy of planetary atmospheres can be used to determine line positions, line strengths, and collisional line widths [8]. Moreover, the values obtained via diode laser spectra are usually among the best available in the literature, demonstrating the wide applicability of the technique [8].

II. APPARATUS

Our experimental apparatus was arranged in two different configurations depending on which quantity we were measuring (Figures 2 and 3). In both cases, we grouped the equipment into four distinct categories. Although we described them individually in this section, it is crucial that they work together as a system, and that different pieces of equipment agree in terms of positioning and alignment.

A. Laser Diode

The light source used for this experiment is a Sanyo DL-7140-201S infrared laser diode. It can be regulated by both temperature and current to reach a maximum power of 70 mW. The nominal wavelength of the laser is 785 nm, but we need to sweep over a range of wavelengths for this experiment. To do that, a diffraction grating is placed at an angle in front of the laser. With correct alignment, the beam diffracted from the grating is sent back to the diode source, creating an "external cavity" that further stabilizes the laser. The grating is mounted on top of a piezoelectric stack, which allows precise control of the grating position and, as a consequence, of the laser frequency. Throughout the experiment, laser temperature was kept constant with the help of a PID controller, and we adjusted the current to fine-tune the laser frequency and maximize the amount of absorption by the Rb gas.

B. Laser Diode Controller

The TeachSpin Laser Diode Controller provides various useful features for the spectroscopy measurements. Beyond the basic capabilities of piezo control, laser temperature and current control, it has two other modules:

1. Ramp Generator module: Provides a bipolar variable amplitude and frequency triangle wave. In our experiment, this was used to modulate the piezo controller and the laser current. The reason why we modulate both is that modulating only the piezo gives rise to "mode hops" as the external cavity and internal diode cavity get misaligned. To fix the alignment (i.e. make sure the laser travels an integer number of wavelengths between the two), we need to adjust the internal cavity as well (in this case, using current modulation).

2. Detector / Low Pass / DC Level module: Provides power for three photodiode detectors, and the ability to combine their signals using different balance factors for each. This module also contains a low-pass filter with time constant ranging from 10 µs up to 0.1 s, a constant DC offset capability, and a way to further adjust the gain of the detectors.

C. Absorption Cell Assembly

A rubidium vapor cell was positioned in the path of probe and pump beams. It sat within a Helmholz coil which was connected to a DC power supply, producing an applied magnetic field at currents up to 4.00 A. The magnetic field was increased at integer steps when measuring the polarization's rotation through the Faraday rotation angle.

A CCD camera was used throughout to qualitatively determine whether or not the Rb atoms were observably at resonance. This camera was connected to a TV monitor.

D. Photodiode Detectors and Optical Devices

After the laser's beam passed through an aperture, it was diverted with a 10:90 BS. The weak path was directed into a Michelson interferometer and the stronger path traveled through a series of optical filters. Another

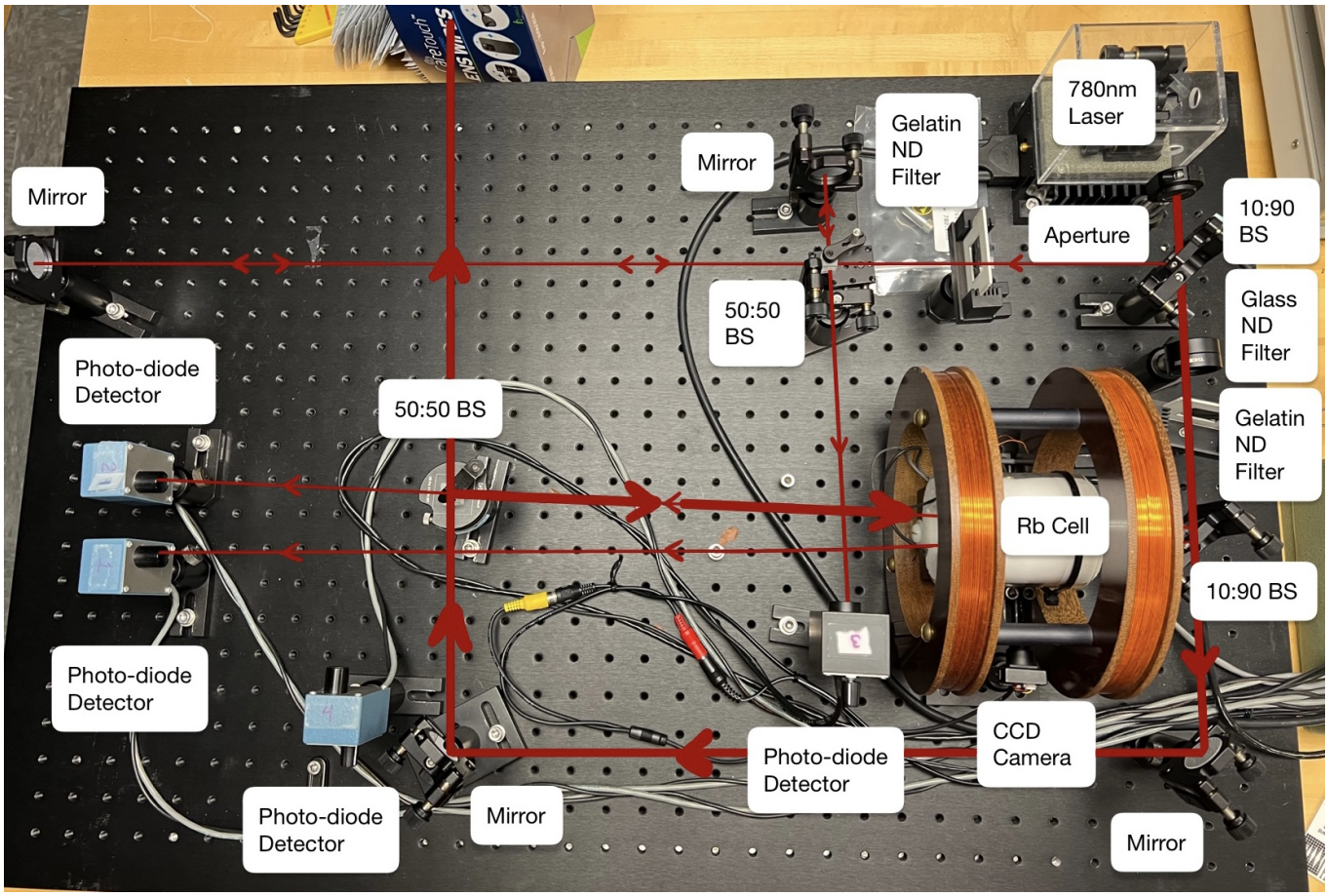

FIG. 2: Experimental setup used for the Saturated Absorption measurements.

10:90 BS was placed along this stronger path. The weaker part of the beam was bifurcated into two paths through the Rb cell. One of these, the "probe," was directed into a 50:50 BS before colliding with photodetector 1. The second went directly to a photodetector 2. The stronger part of the beam, or the "pump," traveled around the Cell and into the same 50:50 BS on the other side. Until the probe and pump overlapped, the pump's path was adjusted by slight modifications to the 50:50 BS and the two mirrors directing it there. This setup was used for saturated absorption spectroscopy. Photodetector 1 was used to measure the absorption spectra of the Rubidium.

The purpose of the bifurcated beams is to isolate the saturated absorption features of the probe beam. By combining the outputs of detectors 1 and 2 and subtracting out the doppler broadening, this is achieved. The Michelson interferometer's beam travels to a third photodetector next to the Rb cell. This signal is helpful for measuring the hyperfine splitting of rubidium. By using an oscilliscope, the interference pattern can be superimposed on that of the saturation absorption spectra to produce cleaner results.

For measuring the polarization's rotation in the presence of a magnetic field, the pump path was no longer necessary. The 50:50 BS was replaced by a polarized beam splitting cube, and photodetectors intersected the two output beams. A polaroid was placed in front of the beam before it entered the Rb cell. Between the beam splitting cube and the cell, a 1/2-waveplate was placed. Once the detectors were connected to an oscilloscope, the 1/2-wavelplate rotated the axis of the beams by $\phi = 45^o$. This was done for several frequencies in the absence of an applied B-field (no Faraday rotation) and made the amplitudes of both beams equal. Afterwards several currents were applied to the Helmholtz coils. Measurements were taken by readjusting the beams so that their amplitudes aligned at the given frequency of the trial. This process occurr for across frequencies.

III. MEASUREMENTS AND DATA ANALYSIS

A. Absorption Spectrum

To measure the frequency separation between the different Doppler broadened absorption features of Rubidium, we used a Michelson interferometer with two legs of length $L_1 = 6 \pm 1$cm and $L_2 = 53 \pm 1$cm. Assuming plane wave propagation (wavenumber k), we see that the phase

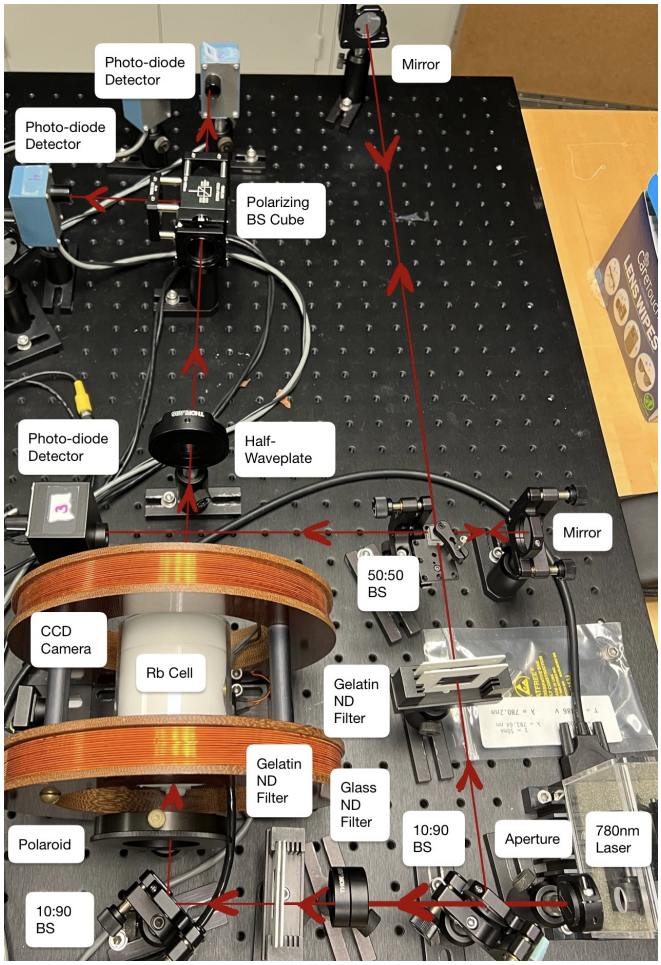

FIG. 3: Experimental setup used for the Faraday Rotation measurements.

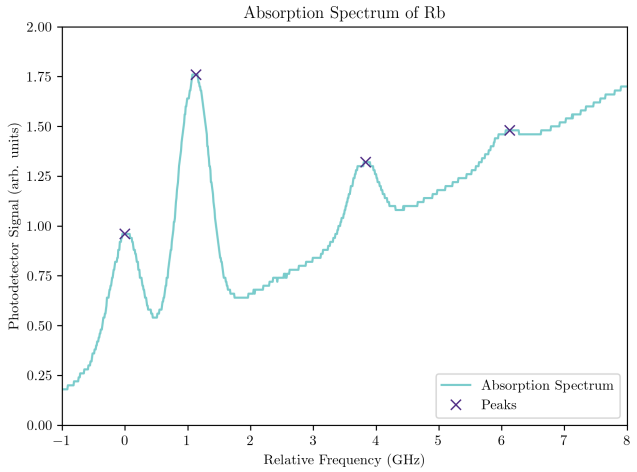

FIG. 4: Typical Doppler broadened absorption spectrum observed in our experiment. We can see that the resolution of the oscilloscope also plays a role in how accurate we can get. From left to right we have: ^{87}Rb F = 2→F', ^{85}Rb F = 2→F', ^{85}Rb F = 3→F', and ^{87}Rb F = 3→F'

TABLE I: Absorption frequency for the different Doppler broadened features.

Feature	Mean Rel. Freq. (GHz)
^{87}Rb F = 2→F'	0
^{85}Rb F = 3→F'	1.13 ± 0.06
^{85}Rb F = 2→F'	4.03 ± 0.08
^{87}Rb F = 3→F'	6.46 ± 0.06

factors acquired by each of the two paths are $\Delta\phi_1 = 2kL_1$ and $\Delta\phi_2 = 2kL_2$. So the phase shift in terms of the laser frequency change Δf is $\Delta\phi = 2(2\pi\Delta f)/(c(L_2 - L_1))$. This means that for a complete cycle of $\Delta\phi = 2\pi$, the equivalent Δf is given by Equation 14.

$$\Delta f = \frac{c}{2(L_2 - L_1)} = 319\text{MHz} \tag{14}$$

While making sure the interferometer was well aligned and the absorption apparatus was tuned to yield maximum absorption, we collected a total of 12 different oscilloscope traces. After that, we calculated the period of the Michelson interferometer oscillations as observed in the oscilloscope. To do that, we fit a sinusoidal model (Equation 15) to each trace over a range of different periods, and then picked the periods that maximized the goodness of the fits (i.e. minimized the χ^2 metric). For evenly spaced data (like ours), this can be proven to be equivalent to analyzing the discrete Fourier transform of the signal as a periodogram[9]. For unevenly spaced data, slight changes in the definition of periodogram make it equivalent to our approach as well [10][11].

$$V = V_0 + A\sin(2\pi P^{-1}(t - t_0)) \tag{15}$$

This process allowed us to analyze the scope traces in the appropriate units of frequency (since we know each oscillation of the interferometer corresponds to $\Delta f =$ 319MHz. We then located the absorption features using a peak finding algorithm and calculated our best estimate for the frequency separation between them as the average over all traces. A typical spectrum (with the peak locations marked) is shown in Figure 4. Results are summarized in Table II.

These measurements agree well with the expected values in the literature.

B. Saturated Absorption Spectrum

Although more complex, the experimental setup used to measured the Saturated Absorption Spectrum (SAS) of Rb is very similar to the one used to measured the Doppler broadened features. We still make use of a

TABLE III: Frequency separation between the various hyperfine transitions.

Feature	Mean Rel. Freq. (MHz)
^{85}Rb F = 3→F'=2	0
Crossover	60 ± 2
^{85}Rb F = 3→F'=3	91 ± 3
Crossover	119 ± 4
Crossover	151 ± 5
^{85}Rb F = 3→F'=4	183 ± 6

Michelson interferometer to know the frequency difference between the various absorption peaks observed. Since it hasn't changed, we still have $\Delta f = 319$MHz and the analysis of the interference pattern is exactly the same as in the previous section. The big difference in this case is that we have a pump beam. This beam is saturating the transitions in such a way that when the frequency is close to the transition frequency, most atoms are in the excited state and the probe beam actually causes stimulated emission (instead of absorption). We were very careful in guaranteeing both beams overlap when going through the Rb cell, otherwise the SAS features can't be seen. We also ensured there were no significant contributions from the interferometer reflecting back.

To collect the data, we subtracted the signals generated by the two photo-diode detectors. Only one of them is being pumped, the other serves simply to help us remove the Doppler broadened background. After fine tuning, we obtained many spectra like that of Figure 5. Then, we used the same peak finding program to find all absorption features, average their frequencies, and take the standard deviation of the sample. The final results are summarized in Table IV.

Because between every pair of real absorption features there must be a "false" crossover feature, we know that the two peaks at the extremities of Figure 5 are real. That also implies the two neighbouring peaks must be crossover features. Finally, we check that the fourth peak is exactly halfway between the two extremities, so it must be false. This makes the third peak a real feature, which (as expected) is consistent with the location of all 6 features (3 of them being real).

This is consistent with what we expect. Because of selection rules, only transitions that respect $\delta m_F = 0, \pm 1$ are allowed. Since we know we are looking at ^{85}Rb, it is easy to label the transitions in the table. In special, we can calculate the energy splittings and compare them with literature values:

C. Faraday Rotation

In order to observe the effects of Faraday rotation, a 1/2-wavelplate was used to align the magnitudes of the output axes of the two beams emitted from the polarized BS cube. After applying an external magnetic field via a Helmholtz coil, the waveplate was used to re-align the magnitudes of the output beams at a given frequency. The change in the angle of polarization required to do this was measured as a function of the current creating the B-field. This was done at 8 different wavelengths of light λ. The resulting shift in polarization angle is described in Table V.

We decided to analyze the validity of Equation 12 by plotting the rotation angle against current (which should be proportional to magnetic field) in Figure 6. Although some were reasonably close to following a linear relationship, there were a few non-linear cases.

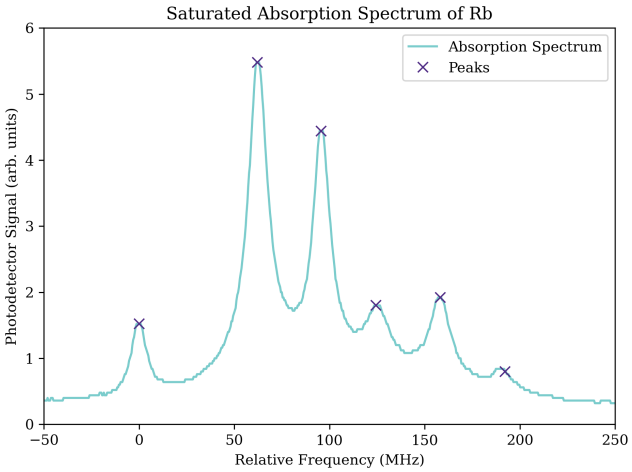

FIG. 5: Saturated absorption spectra for ^{85}Rb F' observed in our experiment. From left to right, the peaks are classified as: real, false, false, real, false, real.

TABLE V: Polarization angles as a function of wavelength λ the applied current through Helmholtz coils.

Polarization Angle vs. Applied Current								
Current (A)	$\theta(\lambda_1, I)$	$\theta(\lambda_2, I)$	$\theta(\lambda_3, I)$	$\theta(\lambda_4, I)$	$\theta(\lambda_5, I)$	$\theta(\lambda_6, I)$	$\theta(\lambda_7, I)$	$\theta(\lambda_8, I)$
0.00	0	0	0	0	0	0	0	0
1.00	-4	-2	12	6	7	2	-4	-4
2.00	-8	-6	18	8	14	4	-6	-6
3.00	-10	-8	26	9	20	6	-8	-6
4.00	-12	-8	30	9	21	6	-10	-8

IV. DISCUSSION

The experiment yielded the typical absorption spectra for the two stable rubidium isotopes. The peaks of fig. 4 reproduce the D_2 transitions ($5S_{\frac{1}{2}} \implies 5P_{\frac{3}{2}}$) according to the prediction of energy level splitting for the S-orbital. Through the use of probe and pump beams, saturated absorption was achieved. Fig. 5 shows the presence of

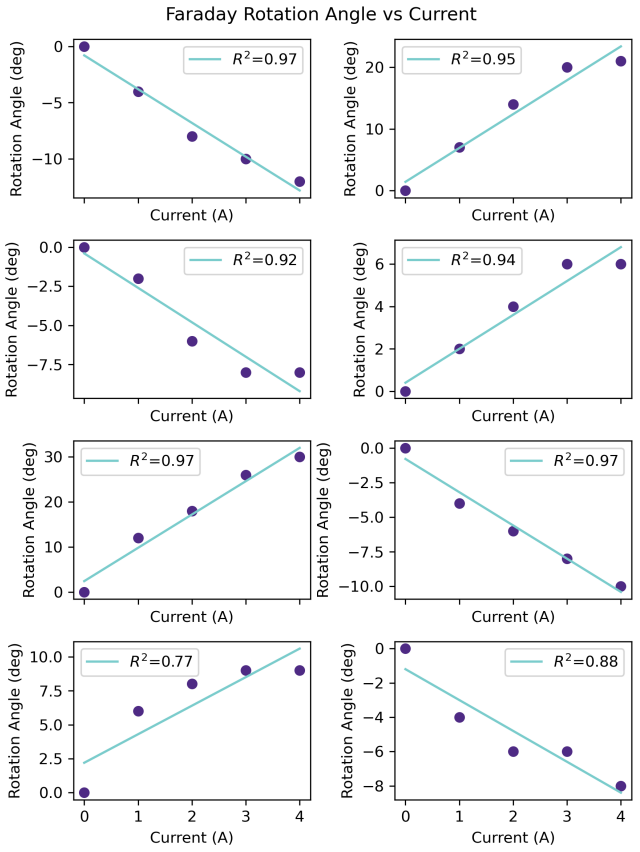

FIG. 6: Best fit lines for all eight different wavelengths. On the left, from top to bottom we have $\lambda_1, \lambda_2, \lambda_3, \lambda_4$. On the right, from top to bottom we have $\lambda_5, \lambda_6, \lambda_7, \lambda_8$.

false peaks consistent with the saturated absorption spectra for hyperfine splittings of ^{85}Rb's F'. One limitation of the experimental apparatus concerned the degree of overlap of the pump and probe beams. The pump was much larger than the probe and overly diverged, making it not as spatially overlapped. This could have decreased the density of saturated states resulting from the pump, increasing the probe's contribution to exciting states and decreasing its transmission at the resonant frequencies to the detector.

At no wavelength was the response to the changing B-field perfectly linear across for all four increases in current. At wavelengths λ_1, λ_6, and λ_7, three out of four consecutive responses to the changing magnetic field were linear. For λ_5 there were two consecutive linear responses. While further investigation must be done to support the notion that the Faraday effect rotates polarization angles linearly, its presence is clearly demonstrated.

Non-linearity in the change of the angle of polarization as a function of B-field and frequency could have resulted from residual saturation. Another contributor could have been changes in absorption from the +/- signals. This can occur in the presence of a changing B-field. Still, the magnitudes by which the angles changed, however, were largely consistent with previous results procured using this specific apparatus (i.e. on the order of | 2 | to | 12 | degrees per 1.00 A).

V. CONCLUSION

Through the use of saturated absorption spectroscopy, the Doppler broadening of the D_2 transitions for a vapor cell of Rubidium was reduced. Saturated absorption was achieved for ^{85}Rb's F', but better overlap of pump and probe beams in our apparatus might have improved the sharpness of these spectra. While Faraday rotation was observed, there was no wavelength for which a purely linear dependence was observed for all changes in the applied B-field. This may have resulted from residual saturation and signal interference from the changing magnetic field. Nonetheless, the magnitude of the obtained results was consistent with previous experiments performed on our experimental apparatus.

[1] Murugesan Balamurugan Chandran Karunakaran. *Spin Resonance Spectroscopy: Principles and Applications*, chapter 4, pages 169–228. Elsevier, 2018.

[2] Daniel A. Steck. Rubidium 87 d line data. *Los Alamos Naitonal Laboratory, Theoretical Division (T-8), MS B285*, 2001 (revised 2003).

[3] Daniel A. Steck. Rubidium 85 d line data. *Oregan Center for Optics and Department of Physics, University of Oregan*, available online at http://steck.us/alkalidata (revision 2.3.2, 10 September 2023).

[4] *User's Manual for Diode Laser Spectroscopy, DLS1-A*. TeachSpin, Inc., Buffalo, NY, Rev. 2.0 11/09.

[5] Thomas Volz Thomas Rieger. Doppler-free saturation spectroscopy. *Max-Planck-Institut fur Quantenoptik, Garching*, available online at https://www.mpq.mpg.de/4992695/saturation_spectroscopy.pdf.

[6] David van Baak. Resonant faraday rotation as a probe of atomic dispersion. *Am. J. Phys.*, 64:724–735, 1996.

[7] Shan Lin, Jun Chang, Jiachen Sun, and Peng Xu. Improvement of the detection sensitivity for tunable diode laser absorption spectroscopy: A review. *Frontiers in Physics*, 10, 2022.

[8] D.E. Jennings. Laboratory diode laser spectroscopy in molecular planetary astronomy. *Journal of Quantitative Spectroscopy and Radiative Transfer*, 40(3):221–238, 1988. Special Issue on Quantitative Spectroscopy and Laser Diagnostics.

[9] Thus, the only reason for doing this is that we felt more comfortable dealing with data in this format, and it seemed easier to catch mistakes.

[10] N. R. Lomb. Least-Squares Frequency Analysis of Unequally Spaced Data. *Astrophysics and Space Science*, 39(2):447–462, February 1976.

[11] J. D. Scargle. Studies in astronomical time series analysis. II. Statistical aspects of spectral analysis of unevenly spaced data. *The Astrophysical Journal*, 263:835–853, December 1982.